Desalination and Water Treatment
www.deswater.com
doi: 10.5004/dwt.2019.24230

158 (2019) 353–363
August

Preparation of granular red mud supported zero-valent iron for Crystal Violet removal from aqueous solution

Yufeng Du[a], Min Dai[b], Jiangfei Cao[b], Jiwei Liu[a], Changsheng Peng[a,b,*]

[a]*The Key Laboratory of Marine Environmental Science and Ecology, Ministry of Education, Ocean University of China, Qingdao 266100, China, Tel./Fax: +86 532 66782011; emails: pcs005@ouc.edu.cn (C. Peng), duyfsdut@126.com (Y. Du), 842922478@qq.com (J. Liu)*
[b]*School of Environmental and Chemical Engineering, Zhaoqing University, Zhaoqing, 526061, China, emails: 1183492590@qq.com (M. Dai), 347582121@qq.com (J. Cao)*

Received 9 November 2018; Accepted 3 April 2019

ABSTRACT

In this study, the granular red mud supported zero-valent iron (GRM@ZVI) was successfully synthesized with bentonite as binder and maize straw as pore former. zero-valent iron (ZVI) was synthesized by direct reduction of iron oxide in red mud with maize straw as reductant at 900°C. The synthesized material was characterized with different methods such as scanning electron microscopy, energy dispersive spectroscopy, X-ray diffraction, Fourier transform infrared spectroscopy, and Brunauer, Emmett and Teller. Various parameters affecting CV removal are as initial dye concentration (100–1,000 mg/L), initial pH (3.0–11.0), dosage (2–1.4 g/L) and temperature (303–323 K) have been investigated in present study. In addition, the three-adsorption kinetics has been employed to study the removal process of CV. The adsorption process was well fitted with the pseudo-second-order kinetic model which indicated that the chemisorption was the rate controlling step and internal particle diffusion controlled in some degrees. The Langmuir model good described the adsorption isotherms indicated the adsorption of CV occurring on a homogeneous surface. According to adsorption kinetics and isotherms, the maximum adsorption capacity of GRM@ZVI for CV was 305.84 mg/g. Summarily, the GRM@ZVI can be prepared as a low cost and effective adsorbent for the removal of dyes from aqueous solutions.

Keywords: Red mud; Crystal Violet; Zero-valent iron; Adsorption; Reduction

1. Introduction

Red mud (RM) is also called bauxite residue, a kind of waste tailing after Bayer alumina production [1]. Because of high alkalinity and large amount, RM causes serious environmental risk which may disrupt the surrounding ecological balance [2]. On average, to produce one ton of alumina, 1.0–2.0 tons of red mud are produced as waste. It is estimated that about 4 billion tons red mud have been produced annually in recent years and it is still rapidly increasing [3]. China is one of the largest producers of alumina in the world, the accumulative inventory of RM has reached more than an estimated 0.6 billion tons [4]. Hence, it is necessary to find a new option for the disposal and management of red mud tailing, at the same time, it is also one of the major challenges facing by the alumina industry [5].

Red mud has good porous structure properties and its surface has an important hydroxyl group, so the use of RM as an adsorbent has been studied, such as heavy metal [6,7], organics [8], and dyes [9] from aqueous solutions. In general, the mineral composition of RM includes various forms of iron, aluminum oxides and aluminosilicates [10]. The high

* Corresponding author.

amount of iron in red mud can be recovered by solid-phase method and be reduced to ZVI. The preparation of ZVI using a solid-phase reduction method has been studied and is a cost-effective method compared with the liquid phase reduction [11,12].

Recently, ZVI has attracted much attention and has been widely used in the field of water treatment due to its high reduction capacity, larger surface area and environmental friendliness. However, ZVI particles tend to aggregate and oxidize in aqueous solution, resulting in a decrease in catalytic ability and, limiting the application of water treatment. In order to solve this problem, researchers have attempted using different porous materials, such as bentonite, kaolinite, activated carbon and biochar, which aims to stabilize ZVI and reduce particle agglomeration [13]. ZVI has been applied to the removal of pollutants in aqueous solutions, including the degradation of dyes. Crystal Violet is a kind of cationic dyes with complex structure and hard degradation. They cause environmental problems and pose a serious threat to public health [14]. The powdered RM and ZVI have been used as adsorbents for CV removal in some studies [15,16]. Because of its disadvantage in regeneration and recovery, the application in water treatment is limited. Therefore, it is necessary and feasible to prepare RM into granular adsorbent. But nowadays there are few studies on preparation of ZVI porous granular adsorbent by solid phrase reduction of red mud.

In this study, the red mud was employed as the main raw material to produce granular adsorbents (GRM@ZVI) to remove CV in aqueous solution. A cost-effective approach was used to prepare ZVI, which was directly synthesized through solid-phase reduction in the anoxic atmosphere. Maize straw was used as a reducing agent at 900°C and ZVI was well distributed in porous adsorption materials [17]. Bentonite and straw were applied as binding agents and aperture producer, moreover, bentonite and straw also effectively generate the gaps during sintering process which can accelerate for the CV adsorption. In addition, the parameters of CV adsorption and characteristics of GRM@ZVI, such as X-ray diffraction (XRD), Fourier transform infrared spectroscopy (FTIR), scanning electron microscopy (SEM) and Brunauer, Emmett and Teller (BET), were also discussed in this study.

2. Experiment

2.1. Materials and chemicals

Red mud (RM) was obtained from Shandong Aluminum Industry Co. Ltd. (Zibo, China). The chemical composition of RM was analyzed through XRF (Table 1), indicating that RM was primarily a mixture of Fe, Al, Si and oxides. Bentonite was obtained from Shandong Huawei Bentonite Co. Ltd. (Qingdao, China). Maize straw was collected from a farmland.

Crystal violet ($C_{25}H_{30}ClN_3$), hydrochloric acid (HCl), sodium hydroxide (NaOH), sulphuric acid (H_2SO_4), potassium dichromate ($K_2Cr_2O_7$), phosphoric acid (H_3PO_4) and ferric chloride hexahydrate ($FeCl_3{\cdot}6H_2O$) were purchased from Tianjin Chemical Reagent Co. Ltd. (Tianjin, China). All the reagents were of analytical grade and distilled water was used in all preparations. The solution pH was adjusted by using HCl and NaOH solutions.

Table 1
Composition of RM used (wt.%)

Constituent	Red mud
Fe_2O_3	45.40
Al_2O_3	21.56
SiO_2	11.93
Na_2O	10.55
TiO_2	6.42
CaO	1.36
K_2O	0.09
LOI	2.69

2.2. Preparation of GRM@ZVI

GRM@ZVI was made by using raw materials with RM, maize straw and bentonite. The RM and bentonite were put in the oven for 24 h at 65°C and ground into a 200-mesh screen, maize straw was cut into small pieces and washed thoroughly with hot distilled water. After being dried at 85°C for 24 h, the pieces were comminuted and sieved through a 100-mesh screen with a micro plant grinding machine. Then GRM@ZVI was prepared with RM, maize straw, and bentonite at mass ratio of 2:1:0.5, added to the blender with the distilled water and mixed for 30 min. The mixture was extruded through an aperture board to get cylindrical particles with diameter of 3.5 mm and the particles were dried at 105°C for 24 h. The granular material obtained before sintering was called GRM. And then, they were sintered in an atmosphere sintering furnace at 900°C with the heating rate of 10°C for 60 min under reducing atmosphere [18]. After naturally cooling down in a vacuum, GRM@ZVI was finally obtained. Schematic diagram of GRM@ZVI preparation is shown in Fig. 1.

2.3. Analytical methods

The microstructure of GRM@ZVI and GRM was characterized by using SEM (JSM-6700F). The elemental composition of GRM@ZVI and GRM was determined by energy dispersive spectroscopy (EDS, JSM-6700F). The BET-N_2 adsorption method was used to test the specific surface area with a surface analyzer (Micromeritics, ASAP 2020, Shanghai). The GRM@ZVI samples chosen for XRD analysis were ground and sieved through a 100-mesh screen. XRD spectroscopy patterns of GRM@ZVI and GRM were analyzed by XRD (D/max-γB). The functional groups of GRM@ZVI were identified using FTIR (Bruker Vertex 70, Beijing). The content of ZVI in GRM@ZVI was measured by ferric chloride leaching-potassium dichromate titration method.

2.4. Batch experiments

A series of removal experiments of CV in aqueous solutions were carried out by using GRM@ZVI. The effect of the contact time was investigated by changing the time from 0.5 to 72 h at 303 K. The effect of initial pH in a range of 3.0 to 11.0 was studied. The pH was adjusted to the desired level with 0.1 M NaOH or 0.1 M HCl solutions. The initial

Fig. 1. Schematic diagram of GRM@ZVI preparation.

concentration from 100 to 1,000 mg/L (100, 200, 400, 600, and 1,000 mg/L) was studied. The dosage (0.2–1.4 g) and temperature (303, 313, and 323 K) on the removal of CV by GRM@ZVI were studied. The obtained data were used to develop kinetic and equilibrium mathematical models. These flasks were shaken at 120 rpm in a shaker. The residual concentration of CV solution was measured using a UV–Vis spectrophotometer at λ_{max} = 585 nm. The removal amount and efficiency of Crystal violet were calculated by the following formula:

$$q_t = \frac{(C_0 - C_t)}{w} \times V \quad (1)$$

$$R = \frac{(C_0 - C_t)}{C_0}\% \quad (2)$$

where q_t (mg/g) is the removal capacity of Crystal violet, C_0 (mg/L) is the initial concentration of Crystal violet, C_t (mg/L) is the concentration of Crystal violet at time t, w (g) is the weight of the adsorbent, V (L) is the volume of the solutions, R (%) is the removal efficiency of the manufactured adsorbent.

3. Results and discussion

3.1. Characterization of GRM@ZVI

The morphology of GRM@ZVI and GRM was characterized by SEM and EDS as shown in Fig. 2. It can be seen clearly that the GRM@ZVI surface was rough and produced a plenty of pores compared with GRM. These pores were produced by the organic substances in the maize straw during the pyrolysis process. In addition, fibrous maize straw can be connected to the closed pores during the pyrolysis process, increasing the specific surface area of adsorbent [19]. This also proved that GRM@ZVI was a porous adsorbent. The EDS image showed that GRM@ZVI was mainly composed of Fe, O, Al, Si and C. The EDS images of GRM@ZVI and GRM are shown in Fig. 2c. It proved that GRM@ZVI was mainly composed of Fe, O, Al, Si, and C. Compared with GRM, the decrease of C and O in GRM@ZVI is mainly due to pyrolysis of organics and decomposition of carbonate and the reduction of combined water.

The XRD spectrum was also used to explore the phase structures of materials. The XRD patterns of GRM@ZVI and GRM are shown in Fig. 3a. The peak at 2θ = 44.64°, 65.166°, 82.378° represented the characteristic peak of ZVI and confirmed its existence in prepared GRM@ZVI. After sintering, the peak of Fe_2O_3 (2θ = 33.06°, 2θ = 35.80°, 2θ = 54.19°) decreased [20]. Meanwhile, this also confirmed that iron oxide was reduced to ZVI by solid-phase reduction in high temperature reducing atmosphere.

The FTIR spectra in the range of 400–4,000 cm^{-1} for GRM@ZVI are presented in Fig. 3b. The two peaks at around 3,450 and 1,643 cm^{-1} were assigned to the stretching vibration of hydroxyl groups and were likely due to the presence of H_2O or hydroxyl compounds in GRM@ZVI [21]. The characteristic band at 1,002 cm^{-1} corresponded to Si–O in the silicate groups [22]. Furthermore, the peaks at 468 and 521 cm^{-1} were observed on Fe–O of Fe_2O_3, indicating that Fe compounds existed in GRM@ZVI. These results and XRD analysis demonstrated that ZVI could be successfully loaded onto the surface of GRM@ZVI.

To study the specific surface area and pore size distribution of GRM@ZVI, BET analysis was used as shown in Fig. 4. According to the IUPAC classification, the nitrogen adsorption–desorption isotherms of GRM@ZVI belongs to a typical type IV with a type H1 hysteresis loop due to the mesoporous pores of GRM@ZVI (Fig. 4a). As shown in Fig. 4b, the pore size distribution curve of GRM@ZVI indicates that the pores in the sample are mainly mesopores (2–50 nm), and a small number of micropores and macropores. According to the results, the specific surface area and average pore size were 44.575 m^2/g and 3.413 nm, respectively.

3.2. Effect of experimental parameters on the removal of CV

The solution pH played an important role in CV removal process. Fig. 5a shows that the effect of initial pH on removal of CV by using GRM@ZVI with initial concentration of 600 mg/L and a dosage of 2.0 g/L. The result showed

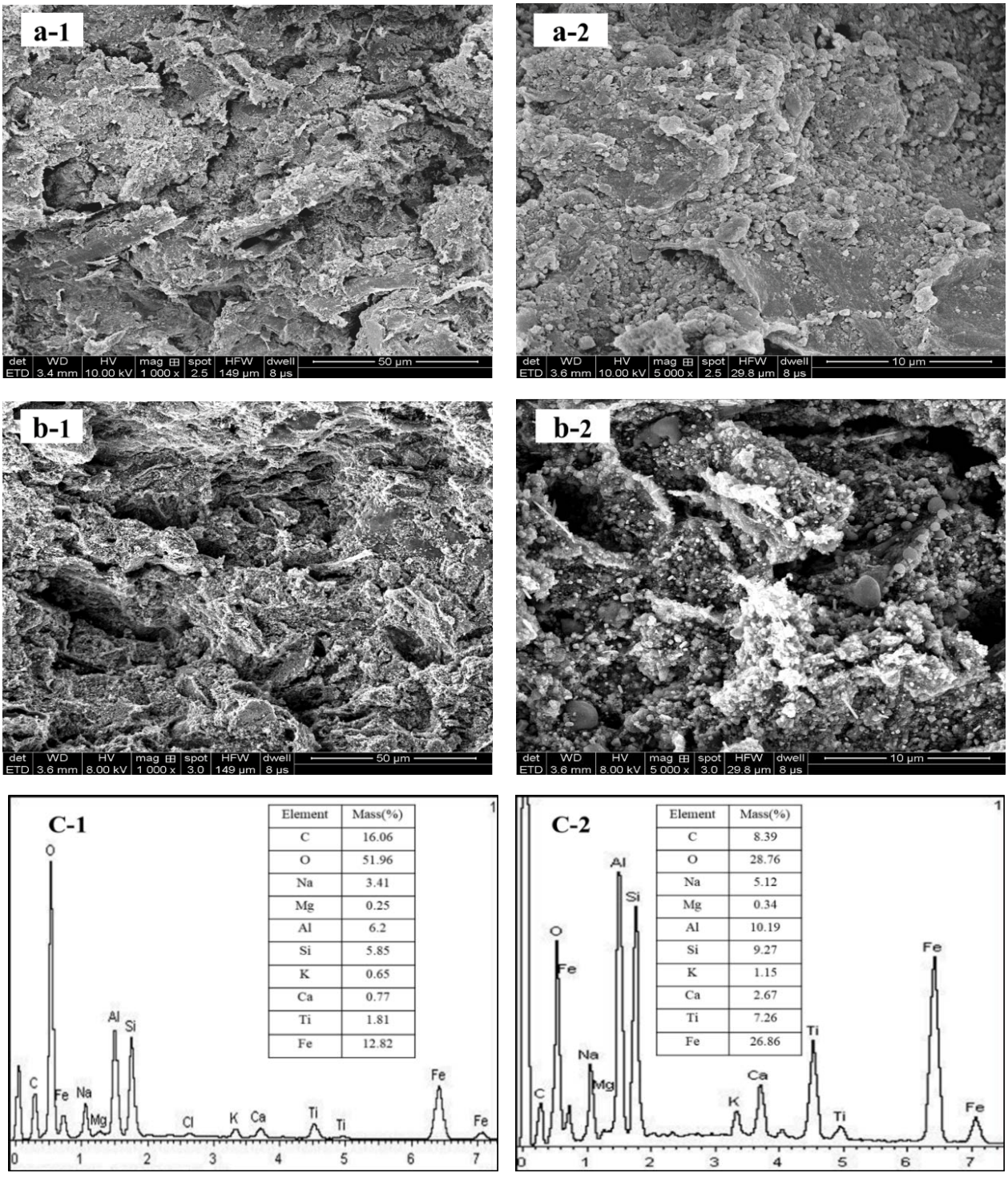

Fig. 2. (a) SEM image of GRM: (a-1) 1,000x and (a-2) 5,000x; (b) SEM image of GRM@ZVI: (b-1) 1,000x and (b-2) 5,000x; (c) EDS image of GRM (c-1) and GRM@ZVI (c-2).

that removal efficiency of CV increased with the increase of pH value from 1.0 to 11.0, which indicated that the removal amount of CV was higher at alkaline condition. The result can be explained by considering the point of zero charge (pH_{pzc}) of GRM@ZVI. The surface charge was positive at $pH < pH_{pzc}$, the surface charge was neutral at $pH = pH_{pzc}$ and negative charge at $pH > pH_{pzc}$ [23]. The surface charge of the material can affect the electrostatic force between the adsorbent and the adsorbate. In this experiment, the point of zero charge of GRM@ZVI was about 5.2. The red mud contains rich metal oxides which can form aqua complexes in aqueous solutions and create a charged surface

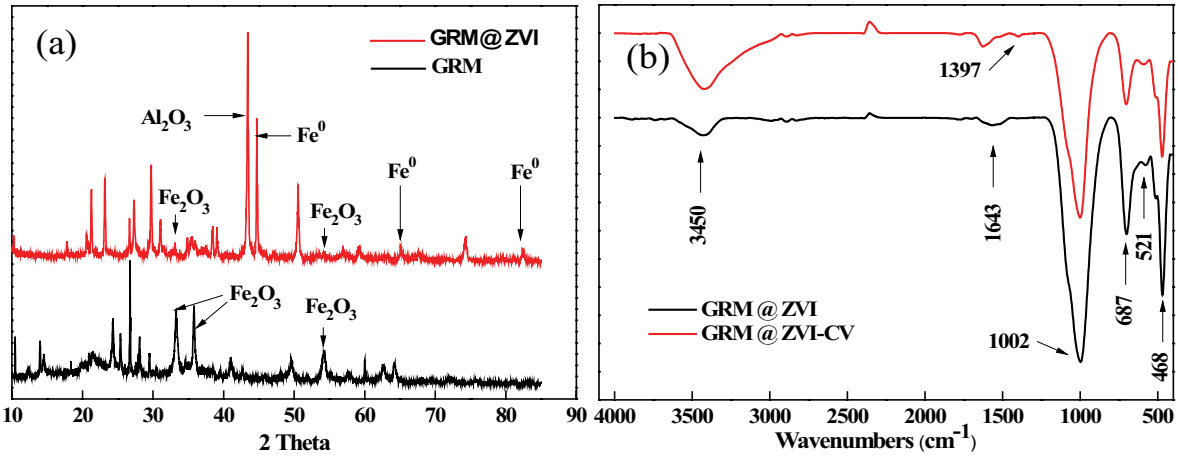

Fig. 3. (a) XRD pattern of GRM@ZVI and GRM and (b) FTIR spectra of GRM@ZVI before and after adsorption CV.

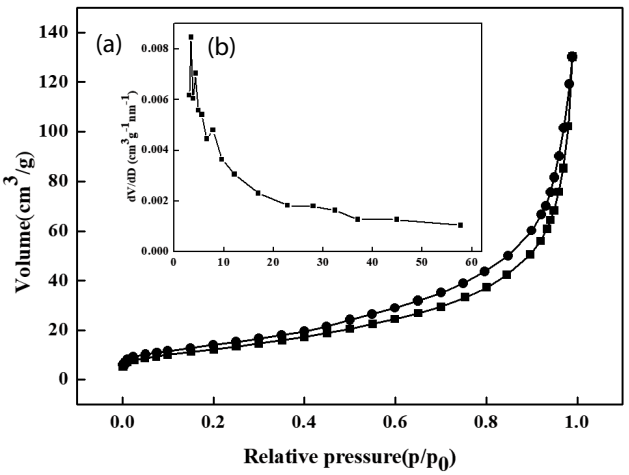

Fig. 4. (a) Nitrogen adsorption–desorption isotherm of GRM@ZVI; (b; inset) pore size distribution of GRM@ZVI.

by amphoteric dissociation. At pH > pH_{pzc}, the surface sites were mostly negatively charged and cationic was easily absorbed due to the electrostatic interaction between GRM@ZVI surface and cationic. At lower pH, the repulsive forces between cationic CV and positive charge of GRM@ZVI surface would hinder the adsorption of CV. Furthermore, the properties and mineralogical composition of red mud would change with pH and the adsorption sites would be relatively lost because of the redundant H^+ in solutions competing with cationic CV at lower pH. However, under the acidic condition, the ZVI dissolved quickly into the bulk solution, which was essential for CV reduction [24]. At higher pH, the precipitation of ferrous hydroxide on the surface of the ZVI occupying the reactive sites stopped the release of ferrous ions and electrons, thus hindering the reaction. Therefore, in this experiment, at higher pH, the adsorption progress played a dominated role than the reduction process.

Furthermore, in order to study different pH on the colour of CV, UV–Vis spectra of CV at different pH are shown in Fig. 5b. The UV–Vis absorbance of CV showed that the absorption peak at 585 nm disappeared with the increase of pH at 1 and 13, and when the pH was in the range of 3–11, the colour had no significant difference. So, the solution pH too high or too low will hinder the reaction.

Fig. 5c shows the effect of initial concentrations ranging from 100 to 1,000 mg/L on the removal of CV with initial pH 5.5 and a dosage of 2.0 g/L. Results indicated that the removal efficiency of CV increased as initial concentration decreased and the removal rate increased sharply at in the initial stage of the reaction. As the reaction progressed, the adsorption rate gradually decreased and tended to equilibrium. For instance, the CV removal amount quickly rose to 46.8 mg/g and nearly achieved 100% removal efficiency during 12 h with the initial concentration of 100 mg/L. Moreover, there was no obvious change after 24 h. While the initial concentration ranges from 100 to 1,000 mg/L, the trend of adsorption and reaction time was invariant. This scenario implied that the removal of CV occurred initially within the first 12 h. Since then, the CV concentration removal was rarely changed. As the initial concentration increased, the removal efficiency gradually decreased, and the time for adsorption to reach equilibrium also increased. The removal rates of CV were 100%, 92.8%, 83.6%, 75.3%, and 61.9%, respectively, with a concentration from 100 to 1,000 mg/L. The reason can be explained as: the removal of CV by GRM@ZVI was a heterogeneous reaction involving adsorption and reduction. Due to the adsorption capacity and reaction site being limited at the fixed GRM@ZVI concentration, an increase in the initial concentration led to competitive adsorption and reduction of CV on GRM@ZVI [17,25].

As shown in Fig. 5d, the removal efficiency of CV rose when the dosage of GRM@ZVI increased. The reason is that the increase of the adsorption dosage led to more zero-valent iron and higher adsorption sites on GRM@ZVI adsorbent which improved the removal efficiency of CV. When the adsorption dosage exceeded 0.8 g, the removal efficiency of CV tended to balance. At this point, the removal efficiency was up to 94.03%. When the dosage of adsorbent is too high, a large number of absorbable sites and zero-valent iron cannot be effectively used and the molecular weight of CV in contaminated water is limited, so the removal of CV did not increase but tended to gradually balance.

3.3. Adsorption kinetics

On the basis of the above results and together with previous reports, it was concluded that the CV removal in

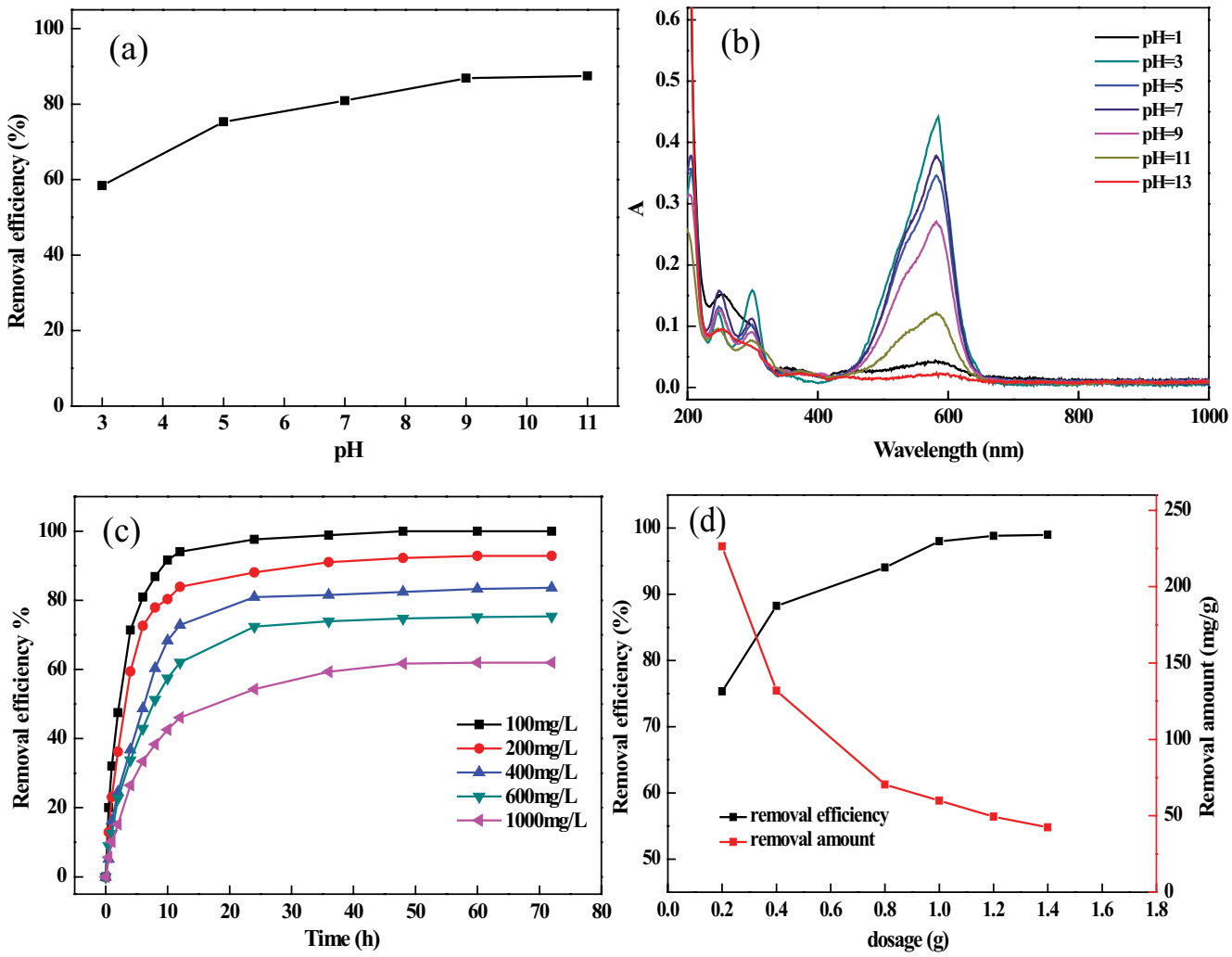

Fig. 5. Effect of (a) pH; (b) UV–Vis spectra at different pH; (c) initial concentration; and (d) GRM@ZVI dosage.

GRM@ZVI involves adsorption and simultaneous chemical reduction. In order to understand the specific dynamics of the removal process, different kinetic models were used to fit the experimental data.

The CV removal in GRM@ZVI involved adsorption and simultaneous chemical reduction. Different kinetic models were used to understand the specific dynamics of the removal process. Pseudo-first-order, pseudo-second-order kinetic model and the intra-particle diffusion theory have generally been used to establish the kinetics of CV adsorption onto GRM@ZVI. The kinetics equation can be expressed as:

The pseudo-first-order kinetics [26]:

$$\ln\left(q_e - q_t\right) = \ln q_e - k_1 t \tag{3}$$

The pseudo-second-order kinetics [27]:

$$\frac{t}{q_t} = \frac{1}{k_2 q_e^2} + \frac{t}{q_e} \tag{4}$$

The intra-particle diffusion [28]:

$$q_t = k_p t^{\frac{1}{2}} + C \tag{5}$$

where q_e and q_t (mg/g) are the adsorption amounts of CV adsorbed on the adsorbent at equilibrium and at different times t. k_1, k_2, and k_p are the rate constant of first and second order kinetic models and intra-particle diffusion model in h^{-1}, g(mg h)$^{-1}$, and mg/g $h^{½}$, respectively.

The kinetic parameters for the adsorption of CV are listed in Table 2. Known by the correlation coefficient R^2 of kinetic model, pseudo-second-order model had a better description of CV adsorption than pseudo-first-order model. In contrast, the pseudo-second-order model contained the processes of adsorption, such as external liquid membrane diffusion, surface adsorption and intra-particle diffusion, which more truly reflects the adsorption mechanism of dyes on GRM@ZVI. Moreover, the value of q_e (333.33 mg/g) calculated from the pseudo-second-order kinetics model was in good agreement with experimental value of

Table 2
Kinetic parameters for the adsorption of CV

Concentration (mg/L)		100	200	400	600	1,000
Pseudo-first-order model	q_e (mg/g)	23.59	48.16	107.82	169.85	283.95
	k_1 (h^{-1})	0.1177	0.0959	0.089	0.0984	0.102
	R^2	0.8936	0.9415	0.95	0.9836	0.9658
Pseudo-second-order model	q_e (mg/g)	51.28	95.24	181.81	243.90	333.33
	k_2 (g mg^{-1} h)	0.011419	0.00419	0.001146	0.000836	0.000536
	R^2	0.9997	0.9995	0.9963	0.9978	0.9984
Intra-particle diffusion model	k_p (mg/g $h^{0.5}$)	4.16	8.5796	18.721	25.304	35.572
	C	22.757	34.873	41.434	53.787	56.59
	R^2	0.6245	0.6652	0.7574	0.8036	0.8635

q_e (305.84 mg/g) at 303 K. Therefore, this demonstrated that chemisorption rather than physi-sorption was the rate controlling step throughout most of the adsorption process.

The pseudo-first-order and pseudo-first-order kinetic models only described the adsorption progress without identifying the diffusion mechanism. Therefore, the intra-particle diffusion model usually describes particle diffusion and with three adsorption steps. As shown in Fig. 6, in this form, the first adsorption step was the external surface adsorption or instantaneous adsorption stage; the gradual adsorption stage occurred in the second part, where the intra-particle diffusion rate was controlled; the third step was the final equilibrium step, where the intra-particle diffusion begins to balance with the concentration decrease in solution [29]. As the plot of q_t against $t^{0.5}$ had a deviation from the origin, indicating that intra-particle diffusion affected in controlling adsorption progress [30]. Therefore, the whole process of adsorption was mainly controlled by chemical adsorption, and also controlled by a certain degree of internal particle diffusion.

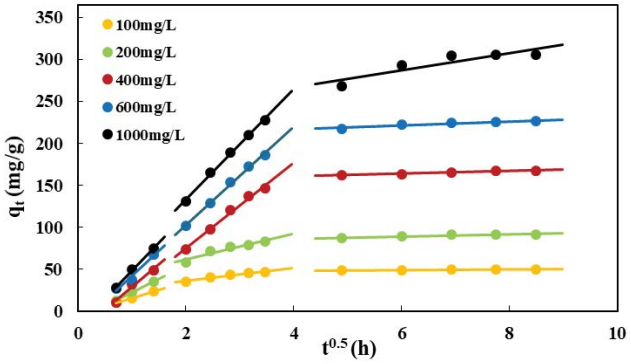

Fig. 6. Intra-particle diffusion model for the adsorption of CV.

3.4. Adsorption isotherms

The equilibrium sorption isotherm is important in the design and analysis of sorption systems and is used to explain the relationship between adsorbent and adsorbate. In this study, the equilibrium sorption data were evaluated by Langmuir, Freundlich, and Temkin isotherms model. The Langmuir model proposed that the adsorption progress on a solid surface occurs in a monolayer and the adsorption sites are of equivalent energy. On the contrary, the Freundlich isotherm is described as assuming that the adsorption occurs on a heterogeneous surface and non-uniform distribution of the adsorption heat over the adsorbent surface takes place [31]. The Temkin isotherm described that the adsorption heat of the molecules in the layer decreased linearly with coverage. The equations can be expressed as:

The Langmuir isotherm model [32]:

$$\frac{C_e}{q_e} = \frac{1}{bq_m} + \frac{C_e}{q_m}$$
$$R_L = \frac{1}{1+bC_0} \quad (6)$$

The Freundlich isotherm model [33]:

$$\ln q_e = \ln k_f + \frac{1}{n}\ln C_e \quad (7)$$

The Temkin isotherm model [34]:

$$q_e = \frac{RT}{b_T}\ln A + \frac{RT}{b_T}\ln C_e$$
$$B = \frac{RT}{b_T} \quad (8)$$

where C_e (mg/L) denotes the equilibrium concentration of CV, q_e (mg/g) is the adsorption amount at equilibrium (mg/g), q_m (mg/g) is the maximum adsorption capacity and b, K_f, and b_T are the Langmuir constant. A is the equilibrium binding constant, R is the gas constant (8.314 J/mol K). R_L describes the characteristic of the Langmuir isotherm with four probabilities, favourable adsorption ($0 < R_L < 1$), unfavourable adsorption ($R_L > 1$), linear adsorption ($R_L = 1$), and irreversible adsorption ($R_L = 0$).

The data of CV adsorption isotherm adsorbed on GRM@ZVI were shown in Table 3. It showed that the correlation coefficient R^2 of Langmuir model was higher than that of Freundlich and Temkin models, which suggested the

Table 3
Isotherms parameters for the adsorption of CV

Temperature (K)		303	313	323
Langmuir	R^2	0.9912	0.9959	0.9979
	q_m (mg/g)	344.83	357.14	454.55
	b (L/mg)	0.0173	0.0348	0.0180
	R_L	0.05–0.37	0.03–0.22	0.05–0.36
Freundlich	R^2	0.9906	0.9968	0.9642
	K_f	43.768	47.404	56.849
	$1/n$	0.3225	0.3641	0.3483
Temkin	R^2	0.9023	0.9885	0.9481
	B (L/mg)	43.28	62.747	56.526
	A (mg/L)	1.342	0.7997	1.8092

Langmuir models well described the adsorption of CV on GRM@ZVI. In addition, the values of q_e (344.83 mg/g) calculated by Langmuir model was corresponding to the q_e (333.33 mg/g) of the pseudo-second-order model. Therefore, the adsorption of CV was monolayer uniform adsorptions on a homogeneous surface. Specifically, q_m and k_f increased with the temperature increasing, which indicated that adsorption of CV was endothermic. The value of q_m, and k_f was 344.83, 357.14, 454.55 mg/g and 43.768, 47.404, 56.849 at 303, 313, and 313 K, respectively. In addition, the values of the separation factor (R_L) were $0 < R_L < 1$ from 0.03 to 0.37, and the temperature ranged from 303 to 323 K, respectively, it indicated that the CV adsorption on GRM@ZVI was favourable and suitable. It can be concluded from these results that GRM@ZVI had extraordinary ability in scavenging CV from the contaminated water.

3.5. Toxicity of GRM@ZVI

Red mud is a kind of solid waste from alumina production, which contains a variety of metal elements and oxides. Using it as an adsorbent to remove contaminants in aqueous solutions may cause potential risk. Measuring the concentration of heavy metals in the lixivium aimed to inspect the toxicity of GRM@ZVI, and their concentrations are shown in Table 4. According to the test standard of Hazardous Wastes Distinction Standard-Leaching Toxicity Distinction (GB 5085.3-2007, China) [35] and State Environmental Protection Administration of China (GB 3838-2002, China) [36], it showed that all heavy metal concentrations in lixivium of GRM@ZVI were much lower than the threshold value. Consequently, GRM@ZVI in the removal progress did not release heavy metal ions and it was considered safe to be applied in wastewater treatment.

3.6. Comparison of different adsorbents for CV removal

Table 5 summarizes the maximum adsorption capacity of various adsorbents for CV removal. The results show that the maximum removal capacity of GRM@ZVI for CV was 305.84 mg/g and it was higher than other analogous adsorbents. In addition, the GRM@ZVI was quite a low-cost material made from red mud, bentonite, and straw as raw materials. Thus, GRM@ZVI was promising in wastewater treatment industry.

3.7. Removal mechanisms

The degradation mechanism of CV from aqueous solution by GRM@ZVI involved the adsorption of CV by porous media and reduction by Fe^0 on GRM@ZVI. As shown in Fig. 7a, the reaction between GRM@ZVI and CV in solutions involved three steps. First, CV molecules were evenly distributed on the surface of GRM@ZVI in solutions. After that they migrated from the surface of GRM@ZVI and diffused into interior pores according to intra-particle diffusion model. Finally, CV was partly reduced to $C_{17}H_{21}N_2$ and $C_8H_{11}N$ by Fe^0 and the adsorption process reached equilibrium. The reaction progress of CV with Fe^0 can be described as shown in Fig. 7b.

Furthermore, Fig. 7c reveals the changes in XRD patterns of GRM@ZVI during the reaction with CV. The result showed that the peaks of ZVI disappeared at $2\theta = 44.64°$, 65.166°, 82.378°, demonstrating that ZVI was oxidized by CV in solution. At the same time, the peaks of Al_2O_3 at $2\theta = 43.406°$ were still discovered before and after reaction with CV, so it was summarized that Al_2O_3 did not participate in the reaction process. In order to further explore the

Table 5
Comparison of the maximum adsorption of CV at different adsorbents

Adsorbents	q_m (mg/g)	Reference
GRM@ZVI	305.84	Present study
Acid-treatment red mud	60.5	[15]
Fly ash-based adsorbent supported ZVI	172.4	[17]
Multifunctional kaolinite-supported ZVI	181.8	[37]
NaOH-modified rice husk	44.87	[38]
Multiwalled-carbon nanotubes	90.52	[39]
Modified magnetic nanoparticles (MNPs)	166.7	[40]

Table 4
Concentrations of heavy metal (mg/L)

Heavy metal	As	Cd	Cr	Cu	Hg	Ni	Pb	Zn
Concentrations in lixivium	0	0	0	0.02	0	0	0	0.11
Limit value	5	1	15	100	0.1	5	5	100
Concentrations in solution	0	0	0	0.01	0	0	0	0.03
Environmental quality standard – level III	0.05	0.005	0.05	1	0.0001	–	0.05	1

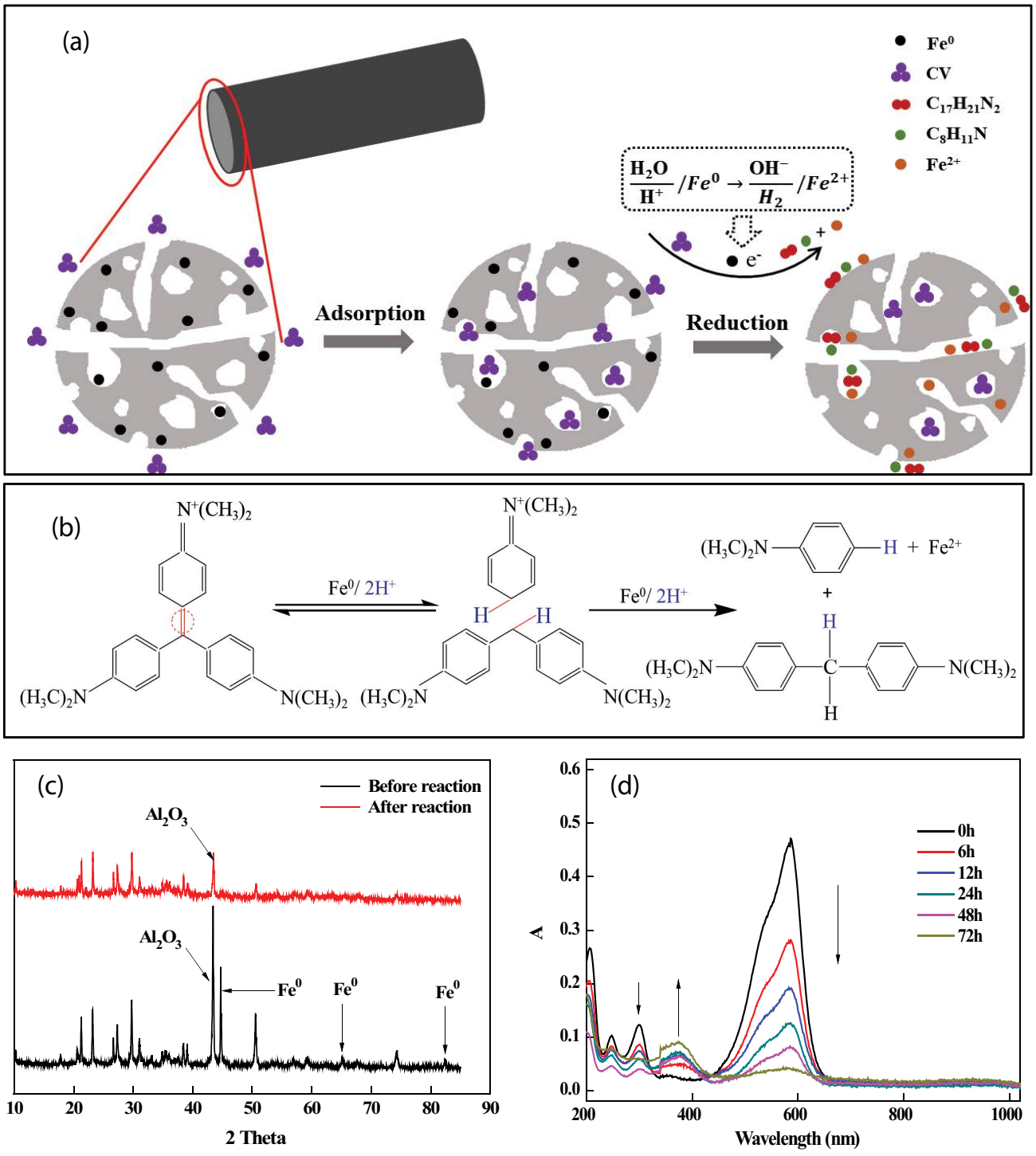

Fig. 7. (a) Adsorption processes of CV; (b) diagram of the degradation of CV by Fe^0; (c) XRD patterns of GRM@ZVI before and after reaction; and (d) UV–Vis spectra of CV at different times.

removal mechanisms, the FTIR spectra of GRM@ZVI after adsorption of CV is shown in Fig. 3b. A new peak appeared at 1,397 cm^{-1} due to the vibration of the C=N, indicating that CV was adsorbed on the GRM@ZVI [41]. During the removal process, the change of CV can be expressed by UV–Vis at different times in Fig. 7d. The UV–Vis absorbance of CV showed that with the progress of the reaction, the absorption peak at 585 nm gradually decreased and a new absorption peak appeared at 373 nm, indicating that a new chemical substance was generated. This was due to the fact that CV was reduced by the zero-valent iron in the surface layer of GRM@ZVI.

4. Conclusions

In this study, GRM@ZVI was produced with three raw materials (red mud, bentonite, and maize) and sintered at 900°C, and in the reducing atmosphere it was evaluated according to adsorption capacity on CV. ZVI was synthesized and embedded in the granular porous adsorbent by direct reduction of ferriferous oxides in red mud. SEM, XRD, FTIR, and the batch experiments confirmed the characteristics of GRM@ZVI: (1) variety sizes of pores exist on the surface of the adsorbent material and mainly due to pyrolysis of the straw, (2) the present of ZVI and homodispersed in GRM@ZVI efficiently maintained reactivity, (3) the removal of CV on GRM@ZVI was highly efficient and dominated by chemisorption. From the result, the removal amount of CV by GRM@ZVI increased by increasing contact time, initial concentration, pH, and dosage of GRM@ZVI. Furthermore, the adsorption processes of CV onto GRM@ZVI better matched the pseudo-second-order kinetic model, indicating the adsorption as a chemical interaction process controlled the removal process. In addition, the Langmuir model showed best fit with the present data, which indicated the adsorption of CV occurring on a homogeneous surface. In conclusion, the GRM@ZVI can be used as a potential, effective, and low-cost adsorbent for remediation of dyes from aqueous solutions.

Acknowledgements

The authors would like to acknowledge the support of the State Key Laboratory of Environmental Criteria and Risk Assessment (SKLECRA2013FP12) and the Shandong Province Key Research and Development Program (2016GSF115040).

References

[1] S.G. Xue, F. Zhu, X.F. Kong, C. Wu, L. Huang, N. Huang, W. Hartley, A review of the characterization and revegetation of bauxite residues (Red mud), Environ. Sci. Pollut. Res., 23 (2016) 1120–1132.
[2] H.L. Zhou, D.Y. Li, Y.J. Tian, Y.F. Chen, Extraction of scandium from red mud by modified activated carbon and kinetics study, Rare Met., 27 (2008) 223–227.
[3] S.G. Xue, X.F. Kong, F. Zhu, W. Hartley, X.F. Li, Y.W. Li, Proposal for management and alkalinity transformation of bauxite residue in China, Environ. Sci. Pollut. Res., 23 (2016) 12822–12834.
[4] X.F. Kong, Y. Guo, S.G. Xue, W. Hartley, C. Wu, Y.Z. Ye, Q.Y. Cheng, Natural evolution of alkaline characteristics in bauxite residue, J. Cleaner Prod., 143 (2016) 224–230.
[5] X.H. Ding, G. Xu, M. Kizil, W. Zhou, X.Y. Guo, Lignosulfonate treating bauxite residue dust pollution: Enhancement of mechanical properties and wind erosion behavior, Water Air Soil Pollut., 229 (2018) 214–226.
[6] R.M. Rivera, B. Ulenaers, G. Ounoughene, K. Binnemans, T.V. Gerven, Extraction of rare earths from bauxite residue (red mud) by dry digestion followed by water leaching, Miner. Eng., 119 (2018) 82–92.
[7] C.L. Zhu, Z.K. Luan, Y.Q. Wang, X.D. Shan, Removal of cadmium from aqueous solutions by adsorption on granular red mud (GRM), Sep. Purif. Technol., 57 (2007) 161–169.
[8] M. Lopez-Garcia, M. Martinez-Cabanas, T. Vilarino, P. Lodeiro, P. Rodriguez-Barro, R. Herrero, J.L. Barriada, New polymeric/inorganic hybrid sorbents based on red mud and nanosized magnetite for large scale applications in As(V) removal, Chem. Eng. J., 311 (2017) 117–125.
[9] O. Kazak, Y.R. Eker, I. Akin, H. Bingol, A. Tor, Green preparation of a novel red mud@carbon composite and its application for adsorption of 2,4-dichlorophenoxyacetic acid from aqueous solution, Environ. Sci. Pollut. Res., 24 (2017) 23057–23068.
[10] J. Li, L. Xu, P.P. Sun, P.Y. Zhai, X.P. Chen, H. Zhang, Z.S. Zhang, W.C. Zhu, Novel application of red mud: facile hydrothermal-thermal conversion synthesis of hierarchical porous AlOOH and Al_2O_3 microspheres as adsorbents for dye removal, Chem. Eng. J., 321 (2017) 622–634.
[11] J.W. Liu, T. Mwamulima, Y.M. Wang, Y. Fang, S.X. Song, C.S. Peng, Removal of Pb(II) and Cr(VI) from aqueous solutions using the fly ash-based adsorbent material-supported zero-valent iron, J. Mol. Liq., 243 (2017) 205–211.
[12] E. Petala, K. Dimos, A. Douvalis, T. Bakas, J. Tucek, R. Zbořil, M.A. Karakassides, Nanoscale zero-valent iron supported on mesoporous silica: characterization and reactivity for Cr(VI) removal from aqueous solution, J. Hazard. Mater., 261 (2013) 295–306.
[13] G.Z. Qu, L.Q. Kou, T.C. Wang, D.L. Liang, S.B. Hu, Evaluation of activated carbon fiber supported nanoscale zero-valent iron for chromium (VI) removal from groundwater in a permeable reactive column, J. Environ. Manage., 201 (2017) 378–387.
[14] R. Ahmad, Studies on adsorption of crystal violet dye from aqueous solution onto coniferous pinus bark powder (CPBP), J. Hazard. Mater., 171 (2009) 767–773.
[15] L.Y. Zhang, H.Y. Zhang, W. Guo, Y.L. Tian, Removal of malachite green and crystal violet cationic dyes from aqueous solution using activated sintering process red mud, Appl. Clay Sci., 93–94 (2014) 85–93.
[16] J.W. Liu, Y.M. Wang, X.L. Zhang, Y. Fang, T. Mwamulima, S.X. Song, C.S. Peng, Preparation of Fe@GAC and Fe@GAR and their application for removal of crystal violet from wastewater, Water Air Soil Pollut., 229 (2018) 38–49.
[17] J.W. Liu, Y.M. Wang, Y. Fang, T. Mwamulima, S.X. Song, C.S. Peng, Removal of crystal violet and methylene blue from aqueous solutions using the fly ash-based adsorbent material-supported zero-valent iron, J. Mol. Liq., 250 (2018) 468–476.
[18] Y. Man, J.X. Feng, Effect of iron ore-coal pellets during reduction with hydrogen and carbon monoxide, Powder Technol., 301 (2016) 1213–1217.
[19] M. Ahmad, S.S. Lee, S.E. Oh, D. Mohan, D.H. Moon, Y.H. Lee, Y.S. Ok, Modeling adsorption kinetics of trichloroethylene onto biochars derived from soybean stover and peanut shell wastes Environ. Sci. Pollut. Res., 20 (2013) 8364–8373.
[20] L.N. Shi, X. Zhang, Z.L. Chen, Removal of chromium (VI) from wastewater using bentonite-supported nanoscale zero-valent iron, Water Res., 45 (2011) 886–892.
[21] S.C. Kang, Y.L. Zhao, W. Wang, T.T. Zhang, T.X. Chen, H. Yi, F. Rao, S.X. Song, Removal of methylene blue from water with montmorillonite nanosheets/chitosan hydrogels as adsorbent, Appl. Surf. Sci., 448 (2018) 203–211.
[22] Z.P. Hu, Z.M. Gao, X. Liu, Z.Y. Yuan, High-surface-area activated red mud for efficient removal of methylene blue from wastewater, Adsorpt. Sci. Technol., 36 (2017) 1–18.
[23] A. Tor, N. Danaoglu, G. Arslan, Y. Cengeloglu, Removal of fluoride from water by using granular red mud: batch and column studies, J. Hazard. Mater., 164 (2009) 271–278.
[24] H.Y. Shu, M.C. Chang, C.C. Chen, P.E. Chen, Using resin supported nano zero-valent iron particles for decoloration of Acid Blue 113 azo dye solution, J. Hazard. Mater., 184 (2010) 499–505.
[25] X.W. Liu, Z.W. Chen, Z.L. Chen, M. Megharaj, R. Naidu, Remediation of Direct Black G in wastewater using kaolin-supported bimetallic Fe/Ni nanoparticles, Chem. Eng. J., 223 (2013) 764–771.
[26] Y.Y. Chen, D.J. Zhang, Adsorption kinetics, isotherm and thermodynamics studies of flavones from Vaccinium Bracteatum Thunb leaves on NKA-2 resin, Chem. Eng. J., 254 (2014) 579–585.
[27] J.P. Simonin, On the comparison of pseudo-first order and pseudo-second order rate laws in the modeling of adsorption kinetics, Chem. Eng. J., 300 (2016) 254–263.

[28] F.C. Wu, R.L. Tseng, R.S. Juang, Initial behavior of intraparticle diffusion model used in the description of adsorption kinetics, Chem. Eng. J., 153 (2012) 1–8.
[29] H.X. Zhang, Z.W. Niu, Z. Liu, Z.D. Wen, W.P. Li, X.Y. Wang, W.S. Wu, Equilibrium, kinetic and thermodynamic studies of adsorption of Th (IV) from aqueous solution onto kaolin, J. Radioanal. Nucl. Chem., 303 (2015) 87–97.
[30] Y.S. Ho, G. Mckay, Sorption of dye from aqueous solution by peat, Chem. Eng. J., 70 (1998) 115–124.
[31] A. Mittal, J. Mittal, A. Malviya, D. Kaur, V.K. Gupta, Adsorption of hazardous dye crystal violet from wastewater by waste materials, J. Colloid Interface Sci., 343 (2010) 463–473.
[32] A.S. Ozcan, O. Gök, A. Ozcan, Adsorption of lead (II) ions onto 8-hydroxy quinoline-immobilized bentonite, J. Hazard. Mater., 161 (2009) 499.
[33] G.K. Sarma, S.S. Gupta, K.G. Bhattacharyya, Adsorption of Crystal violet on raw and acid-treated montmorillonite, K10, in aqueous suspension, J. Environ. Manage., 171 (2016) 1–10.
[34] M. Ghaedi, A. Ansari, M.H. Habibi, A.R. Asghari, Removal of malachite green from aqueous solution by zinc oxide nanoparticle loaded on activated carbon: kinetics and isotherm study, J. Ind. Eng. Chem., 20 (2014) 17–28.
[35] State Environmental Protection Administration of China, GB 5085.3-2007, Hazardous Wastes Distinction Standard-Leaching Toxicity Distinction, China Environmental Science Press, Beijing, 2007.
[36] State Environmental Protection Administration of China, GB 3838-2002, Environmental Quality Standards for Surface Water, China Environmental Science Press, Beijing, 2002.
[37] Z.X. Chen, T. Wang, X.Y. Jin, Z.L. Chen, M. Megharaj, R. Naidu, Multifunctional kaolinite-supported nanoscale zero-valent iron used for the adsorption and degradation of crystal violet in aqueous solution, J. Colloid Interface Sci., 398 (2013) 59–66.
[38] S. Chakraborty, S. Chowdhury, P.D. Saha, Adsorption of Crystal Violet from aqueous solution onto NaOH-modified rice husk, Carbohydr. Polym., 86 (2011) 1533–1541.
[39] V. Sabna, S.G. Thampi, S. Chandrakaran, Adsorption of crystal violet onto functionalised multi-walled carbon nanotubes: equilibrium and kinetic studies, Int. J. Biol. Macromol., 134 (2016) 390–397.
[40] C. Muthukumaran, M. Thirumarimurugan, Adsorption isotherms and kinetic studies of crystal violet dye removal from aqueous solution using surfactant modified magnetic nanoadsorbent, J. Taiwan Inst. Chem. Eng., 63 (2016) 354–362.
[41] W. Wang, Y.l. Zhao, H.Y. Bai, T.T. Zhang, I.G. Valentin, S.X. Song, Methylene blue removal from water using the hydrogel beads of poly(vinyl alcohol)-sodium alginate-chitosan-montmorillonite, Carbohydr. Polym., 198 (2018) 518–528.